Extended Nijboer–Zernike representation of the vector field in the focal region of an aberrated high-aperture optical system

Joseph J. M. Braat

Optics Research Group, Faculty of Applied Sciences, Delft University of Technology, Lorentzweg 1, NL-2628 CJ Delft, The Netherlands

Peter Dirksen

Philips Research Laboratories, WA-01, NL-5656 AA Eindhoven, The Netherlands

Augustus J. E. M. Janssen

Philips Research Laboratories, WY-81, NL-5656 AA Eindhoven, The Netherlands

Arthur S. van de Nes

Optics Research Group, Faculty of Applied Sciences, Delft University of Technology, Lorentzweg 1, NL-2628 CJ Delft, The Netherlands

Received January 6, 2003; revised manuscript received July 8, 2003; accepted July 25, 2003

Taking the classical Ignatowsky/Richards and Wolf formulas as our starting point, we present expressions for the electric field components in the focal region in the case of a high-numerical-aperture optical system. The transmission function, the aberrations, and the spatially varying state of polarization of the wave exiting the optical system are represented in terms of a Zernike polynomial expansion over the exit pupil of the system; a set of generally complex coefficients is needed for a full description of the field in the exit pupil. The field components in the focal region are obtained by means of the evaluation of a set of basic integrals that all allow an analytic treatment; the expressions for the field components show an explicit dependence on the complex coefficients that characterize the optical system. The electric energy density and the power flow in the aberrated three-dimensional distribution in the focal region are obtained with the expressions for the electric and magnetic field components. Some examples of aberrated focal distributions are presented, and some basic characteristics are discussed. © 2003 Optical Society of America

OCIS codes: 000.3860, 050.1960, 070.2580, 110.2990.

1. INTRODUCTION

The study of the exact field distribution in the focal region of a high-numerical-aperture (high-NA) optical system attracts much attention because of the numerous applications where highly focused fields are used. We mention the study of biological specimens such as living cells, cell nuclei, and genetic material with the use of advanced high-resolution microscopy. High-aperture focused fields are equally used in leading-edge optical lithography operating at a deep UV wavelength such as 193 or 157 nm and using projection systems with an image-side NA as large as 0.90. In optical disk readout, the recently standardized Blu Ray Disc system[1] uses a NA of 0.85 and a wavelength of 400 nm. All these applications require a detailed knowledge of the field distribution in the focal region in order to describe the interaction of the probe with the unknown structure or to accurately predict the exposure in the recording layer[2] (e.g., the photoresist layer in optical lithography).

It is the purpose of this paper to accurately describe the vector field in the focal region, starting with the classical Ignatowsky/Richards and Wolf formulas,[3,4] for the aberration-free case, while maintaining the explicit correspondence between specific properties of the imaging system and the field distribution in the focal region. The standard method to calculate the optical field in the focal region uses a purely numerical evaluation of the various diffraction integrals pertaining to the electric and magnetic field components. Even in the case of an aberration-free optical system, these integrals did not seem to admit an analytic solution. In two recent papers,[5,6] an analytic evaluation of the diffraction integral has been proposed and assessed; this analysis concerned the scalar diffraction integral for a (heavily) aberrated optical system. The method has been termed the "extended" Nijboer–Zernike method because it expands aberration and pupil functions in Zernike series and produces manageable expressions for the scalar field through the focal volume, whereas the expressions in the original Nijboer–Zernike method become awkward outside the focal plane. Although the solution consists of an infinite summation, this summation can be safely truncated when

fulfilling some constraints regarding defocus and NA; these constraints are met in most practical cases. We now go further and show that the extended Nijboer–Zernike approach can also be applied to the more complicated case of an aberrated system with high NA by using the vectorial diffraction formalism. The combined effects of amplitude nonuniformity and aberrations are mapped onto a set of generally complex Zernike coefficients that describe the field distribution in the exit pupil; the field distribution in the focal region shows an explicit dependence on these coefficients. The relationship between the properties of the imaging system and the focal field distribution paves the way for a possible inverse problem solution, viz., the retrieval of the complex pupil function from intensity measurements in the focal region. A first step in this direction has been described in Refs. 7 and 8 for the relatively low-NA (say, below 0.8) scalar problem.

This paper is organized as follows. In Section 2, the representation of the field in the entrance pupil of the optical system is discussed. Some specific field distributions are treated, e.g., purely radial or azimuthal polarization[9] and field distributions with an intrinsic nonzero orbital momentum.[10,11] In Section 3, the field in the entrance pupil, including the radiometric effect, is described in terms of an expansion with the aid of Zernike polynomials. To allow for a general description, we propose a complex set of Zernike coefficients that can adequately represent both amplitude and phase variations of the incident field. In Section 4, we present the field distribution in the focal region in terms of the Zernike coefficients, using the analytic approach for solving the various diffraction integrals. The electric energy density and the Poynting vector are evaluated with the expressions for the electric and magnetic field components. Section 5 has been devoted to some practical examples. In Section 6, we present our conclusions and we formulate some suggestions for further research on the subject of this paper.

2. DESCRIPTION OF THE COMPONENTS OF THE FIELD IN THE PUPIL

In Fig. 1, we have depicted the general situation of an optical system with an entrance pupil S_0 and an exit pupil S_1. The geometrical image plane is found at P_I, and a ray has been drawn, representing the incident and focusing waves in the object and image spaces. The incident wave, generated by a point source in the infinitely distant object plane, produces a planar wave front in the entrance pupil; the amplitude and the phase on the wave front are denoted by the (in general) complex quantities $B^x(\rho, \theta)$ and $B^y(\rho, \theta)$ for x and y polarizations, respectively. The x axis is defined here by the polar angle $\theta = 0$. The components B^x and B^y are needed to describe the general situation when the incident field has been produced by, e.g., a preceding optical system, yielding an arbitrary complex-amplitude distribution in the entrance pupil. While propagating through the optical system, optical transmission and path-length variations over the cross section of the wave will change the quantities B^x and B^y in an identical way. Birefringence effects and polarization-dependent phase jumps at transitions between different optical media give rise to changes that are different for B^x and B^y. The polar coordinates (ρ, θ), together with the constant axial coordinate z, are used to describe the field components on the entrance pupil plane S_0; also, the field components on the exit pupil sphere S_1 are described with the aid of the polar coordinates (ρ, θ), together with the nonconstant axial coordinate z. In both cases, we normalize the radial coordinate with respect to the radii a_0 and a_1 of the images of the diaphragm in object and image space that define the circular borders of the entrance and exit pupils. In the image plane, we use the cylindrical coordinates (r, ϕ, f) with $f = 0$ at the geometrical image plane location. Regarding the properties of the optical system, we suppose that it satisfies Abbe's sine condition[12] and that, as stated above, the object plane is located at infinity. Most optical systems obey Abbe's sine condition very closely (e.g., better than 0.1%) because this is a minimum requirement for an aberration-free extended image field. The sine condition for a system with a limited amount of spherical aberration is well approximated by the expression

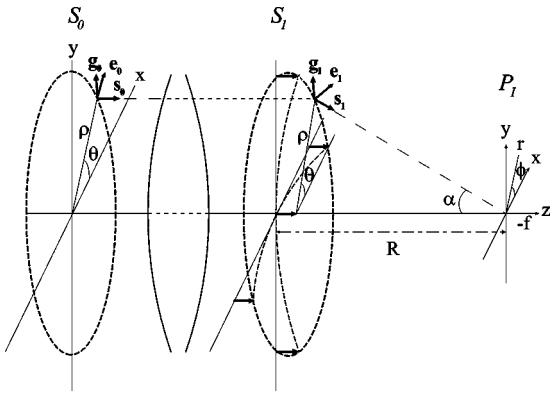

Fig. 1. Propagation of the incident wave from the entrance pupil S_0 through the optical system toward the exit pupil S_1 and the focal region at the image plane P_I. The incident wave has a planar wave front. The unit propagation vector has been denoted by $\mathbf{s}_0$, and the meridional and tangential field components are directed along, respectively, the unit vectors $\mathbf{e}_0$ and $\mathbf{g}_0$. After propagation through the optical system, the field components in the exit pupil are projected onto the unit vectors $\mathbf{e}_1$ and $\mathbf{g}_1$, which form an orthogonal basis with the local propagation vector $\mathbf{s}_1$. The position on the exit pupil sphere is defined by means of the cylindrical coordinates (ρ, θ); the position in the image plane region is defined by the cylindrical coordinate system (r, ϕ, f). The maximum aperture (NA) of the imaging pencil is represented by $s_0 = \sin \alpha_{\max}$.

$$\rho_0 = R \sin \alpha, \tag{1}$$

where ρ_0 is the height of incidence of a particular ray on the entrance pupil plane, α is the angle with the optical axis in the image space of the same ray, and R is the radius of the exit pupil sphere.

We follow the analysis given in Ref. 13 to accommodate the most general field distribution that can be encountered in the entrance or exit pupil of an optical system. The general coherent field is written as the superposition of two orthogonal polarization states. In our case, we take the linear polarization states along, respectively, the x and y axes as basic orthogonal states; a general elliptical state of polarization is obtained through a linear su-

perposition of the two basic linear states with relative amplitude weights and a certain phase difference. The electric field components on the entrance pupil along the x and y axes can be written as

$$B^x(\rho,\ \theta) = A^x(\rho,\ \theta)\exp[i2\pi W(\rho,\ \theta)],$$
$$B^y(\rho,\ \theta) = A^y(\rho,\ \theta)\exp[i2\pi W(\rho,\ \theta) + i\epsilon(\rho,\ \theta)], \tag{2}$$

where A^x and A^y are real-valued functions and describe the field strengths in the x and y directions. $W(\rho,\ \theta)$ is also real valued and describes the wave-front aberration in units of λ, the wavelength of the light, due to optical path-length variation common to both polarization states. The angle $\epsilon(\rho,\ \theta)$ is the spatially varying phase difference that we have chosen to appear in the y component. Nonzero values of ϵ are caused by birefringence in the optical system or by polarization-dependent phase jumps at discontinuities in the optical system (e.g., air–glass transitions, optical surface coatings, etc.). Note that ϵ can be restricted to the range $[-\pi, +\pi]$.

As mentioned above, uniform values of A^x, A^y, and ϵ lead to a uniform polarization state of, in general, an elliptical nature. For various reasons, some other polarization distributions have recently attracted much attention, viz., radial and azimuthal polarization distributions,[9] or, more generally, cylindrical distributions. In terms of the linear polarization states, we write these distributions as

$$B^x = A_0\cos(\theta + \theta_0),$$
$$B^y = A_0\sin(\theta + \theta_0)\exp(i\epsilon) \tag{3}$$

for the radially ($\theta_0 = 0,\pi$) or azimuthally ($\theta_0 = \frac{1}{2}\pi, \frac{3}{2}\pi$) oriented linear ($\epsilon = 0$) polarization state. This combination of x- and y-polarized states leads to a distribution in the pupil as illustrated in Fig. 2.

It is easily shown that a cylindrical distribution of elliptically polarized light is obtained by defining the polarization angle $\epsilon \neq n\pi$, where n equals an integer value. An optical system introducing such a polarization distribution imparts orbital angular momentum to the incident wave; this momentum is preserved and should be detected in the image plane.

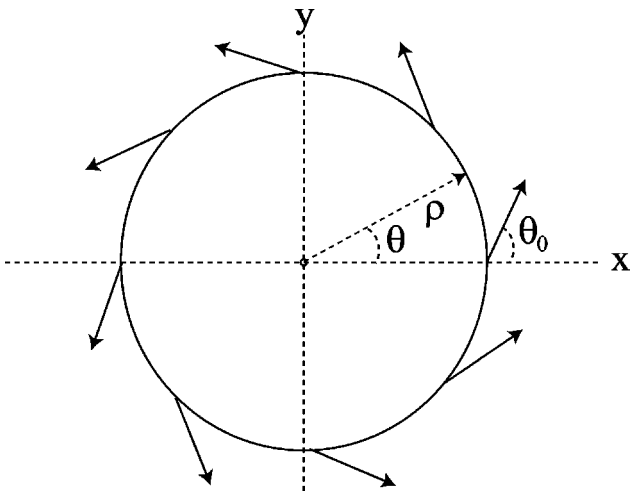

Fig. 2. Distribution of polarization states over, e.g., the entrance pupil for a certain value of the coordinate ρ. The angle ϵ is constant over the pupil and equals zero; $\theta_0 = \frac{1}{3}\pi$.

3. RADIOMETRIC EFFECT AND ZERNIKE EXPANSIONS

An essential ingredient in our method for the computation of the field components in the focal region is the Zernike expansion of aberrations in which the radiometric effect is properly accounted for. The radiometric effect appears in an aplanatic optical system, conjugated at infinity on the object side, that obeys Abbe's sine condition [see Ref. 14, Subsec. 8.6.3(b)]. As a consequence, the modulus of the complex amplitude in the exit pupil contains an intrinsic factor involving the numerical aperture $\mathrm{NA} = \sin\alpha = s_0$ and a factor $B(\rho,\ \theta)$ that is specific for the pupil filling at the entrance of the optical system and for its transmission properties. Note that the pupil function has been described here in terms of the polar coordinates (ρ, θ), where ρ is the perpendicular distance of a point on the exit pupil sphere (radius R) to the optical axis. The intrinsic factor is given explicitly as $(1 - s_0^2\rho^2)^{-1/4}$, i.e., the aberration factor $B(\rho,\ \theta)$ should be divided by the square root of a cosine. Had we used spherical coordinates (ζ, θ) for denoting a general point on the pupil sphere, the radiometric factor due to the sine condition would appear as $\sqrt{\cos\zeta}$ in the numerator.

We thus expand for the x-polarized field component,

$$\frac{B^x(\rho,\ \theta)}{(1 - s_0^2\rho^2)^{1/4}} = \frac{A^x(\rho,\ \theta)}{(1 - s_0^2\rho^2)^{1/4}}\exp[i2\pi W(\rho,\ \theta)]$$
$$= \sum_{n,m}\beta_{nm}^x R_n^{|m|}(\rho)\exp(im\theta), \tag{4}$$

where the summation is over all integer n, m with $n - |m| \geq 0$ and even. We refer to Ref. 14 (Sec. 9.2 and Appendix VII) for general information about the Zernike polynomials $R_n^{|m|}(\rho)$ and their use in the theory of optical aberrations. We may point out here that we use Zernike expansions involving the complex exponential $\exp(im\theta)$, integer m, rather than expansions involving the real trigonometric functions $\cos(m\theta)$, $\sin(m\theta)$, integer $m \geq 0$. The latter type of expansion is appropriately used when the real phase function $W(\rho,\ \theta)$ is to be expanded into a Zernike series as in Ref. 14 (Sec. 9.2). Since we expand the full aberration, corrected for the radiometric effect, complex values enter the scene naturally and there is no reason to insist on real expansion functions. The formulas that result in the sequel by using complex exponentials rather than trigonometric functions are more concise and convenient.

The β_{nm}^x in Eq. (4) are given by

$$\beta_{nm}^x = \frac{n+1}{\pi}\int_0^1\int_0^{2\pi}\frac{B^x(\rho,\ \theta)}{(1 - s_0^2\rho^2)^{1/4}}R_n^{|m|}(\rho)$$
$$\times\exp(-im\theta)\rho\mathrm{d}\rho\mathrm{d}\theta, \tag{5}$$

where the factor $n + 1$ in front of the double integral is a consequence of the normalization $R_n^{|m|}(1) = 1$, so that

$$\int_0^1 R_{n'}^{|m|}(\rho) R_n^{|m|}(\rho) \rho \mathrm{d}\rho = \frac{\delta_{nn'}}{2(n+1)}. \tag{6}$$

Similar considerations hold for the y-polarized field component $B^y(\rho, \theta)$, which yields Zernike coefficients β_{nm}^y as in Eq. (5) by replacing B^x by B^y. Note that the Zernike expansion can also include other systematic effects, such as known aberrations of the imaging system or restrictions imposed on the illumination source regarding its dimension.

We now present some examples of Zernike expansions of pupil functions under certain polarization conditions as we have them in Section 5.

(i) For a constant state of polarization and in the absence of aberrations, we have $B^x = B^y = A_0$. Hence

$$\begin{aligned}\beta_{nm}^x &= \beta_{nm}^y \\ &= \frac{(n+1)A_0}{\pi} \int_0^1 \frac{R_n^{|m|}(\rho)}{(1 - s_0^2\rho^2)^{1/4}} \rho \mathrm{d}\rho \int_0^{2\pi} \exp(-im\theta)\mathrm{d}\theta \\ &= 2(n+1)A_0 \delta_{m0} \int_0^1 \frac{R_n^0(\rho)}{(1 - s_0^2\rho^2)^{1/4}} \rho \mathrm{d}\rho. \end{aligned} \tag{7}$$

In Appendix A, we present a numerically tractable form for the remaining integral in Eq. (7).

(ii) For the field distribution described by Eqs. (3), nonuniform x and y components are found. We get (assuming $\theta_0 = 0$, $\epsilon = 0$ and no aberrations, $A^x = A^y = A_0$) in a way similar to that given above:

$$\beta_{n,\pm 1}^x = \mp i \beta_{n,\pm 1}^y = (n+1)A_0 \int_0^1 \frac{R_n^1(\rho)}{(1 - s_0^2\rho^2)^{1/4}} \rho \mathrm{d}\rho, \tag{8}$$

and $\beta_{nm}^x = \beta_{nm}^y = 0$ when $m \neq \pm 1$. For the remaining integral, see Appendix A.

(iii) We consider a linearly increasing phase function, linearly polarized so that for some real parameter a,

$$B^x(\rho, \theta) = B^y(\rho, \theta) = A_0 \exp(ia\theta). \tag{9}$$

We now find that

$$\begin{aligned}\beta_{nm}^x &= \beta_{nm}^y \\ &= (n+1)A_0 \frac{\exp(i2\pi a) - 1}{i\pi(a - m)} \int_0^1 \frac{R_n^{|m|}(\rho)}{(1 - s_0^2\rho^2)^{1/4}} \rho \mathrm{d}\rho, \end{aligned} \tag{10}$$

where the factor $[\exp(i2\pi a) - 1]/i\pi(a - m)$ is to be interpreted as $2\delta_{ma}$ when a is an integer. See Appendix A for the remaining integral. An optical system introducing such a discontinuous phase function imparts orbital angular momentum to the incident wave; this momentum is also preserved and should be detected in the image plane.

4. EXPRESSIONS FOR THE COMPLEX AMPLITUDES OF THE CARTESIAN FIELD COMPONENTS

In this section, we present the basic formulas to be used for the computation of the complex field components E_x, E_y, and E_z in the focal region. Using these components, we can calculate the Poynting vector at an arbitrary point in the focal region. With the aid of the Poynting vector, the energy flow through the focal region is obtained. When we use the expression for the electric field energy density, the image plane exposure is obtained in the case of, for instance, a lithographic projection system, or, alternatively, the spatially varying detector signal is found when a CCD camera is used for detection.

We start by expanding the x-polarized field component of the exit pupil function into a series involving Zernike polynomials [see Eq. (4)], taking the radiometric effect into account. We follow the developments in Ref. 4 for an aberration-free system and make the transformation from spherical coordinates (θ, ϕ) to cylindrical coordinates (ρ, θ) on the exit pupil for calculation of the diffraction integral. Next, we transform the Cartesian coordinate system (x, y, z) into a cylindrical coordinate system (r, ϕ, f) in the focal region. Explicitly, we substitute $\sin\theta = s_0\rho$ and $\cos\theta = (1 - s_0^2\rho^2)^{1/2}$, $\sin\theta(\cos\theta)^{1/2}\mathrm{d}\theta = s_0^2\rho(1 - s_0^2\rho^2)^{-1/4}\mathrm{d}\rho$, and $\mathbf{k}\cdot\mathbf{x} = 2\pi r\rho\cos(\theta - \phi) + (f/u_0)(1 - s_0^2\rho^2)^{1/2}$ into Eq. (2.26) of Ref. 4. Next we perform the integration with respect to θ by using Eq. (2.29) of Ref. 4 to obtain the field components for the general case:

$$\begin{aligned}E_x^x(r, \phi, f) = -i\gamma s_0^2 \exp\left(\frac{-if}{u_0}\right) \sum_{n,m} i^m \beta_{nm}^x \exp(im\phi) \\ \times \int_0^1 R_n^{|m|}(\rho) \exp\left[\frac{if}{u_0}(1 - \sqrt{1 - s_0^2\rho^2})\right] \\ \times \{(1 + \sqrt{1 - s_0^2\rho^2}) J_m(2\pi r\rho) \\ + \tfrac{1}{2}(1 - \sqrt{1 - s_0^2\rho^2}) \\ \times [J_{m+2}(2\pi r\rho)\exp(2i\phi) \\ + J_{m-2}(2\pi r\rho)\exp(-2i\phi)]\}\rho \mathrm{d}\rho, \end{aligned} \tag{11}$$

$$\begin{aligned}E_y^x(r, \phi, f) = -i\gamma s_0^2 \exp\left(\frac{-if}{u_0}\right) \sum_{n,m} i^m \beta_{nm}^x \exp(im\phi) \\ \times \int_0^1 R_n^{|m|}(\rho) \frac{-i}{2} \exp\left[\frac{if}{u_0}(1 - \sqrt{1 - s_0^2\rho^2})\right] \\ \times (1 - \sqrt{1 - s_0^2\rho^2}) \\ \times [J_{m+2}(2\pi r\rho)\exp(2i\phi) \\ - J_{m-2}(2\pi r\rho)\exp(-2i\phi)]\rho \mathrm{d}\rho, \end{aligned} \tag{12}$$

$$E_z^x(r,\phi,f) = -i\gamma s_0^2 \exp\left(\frac{-if}{u_0}\right)\sum_{n,m} i^m \beta_{nm}^x \exp(im\phi) \times \int_0^1 R_n^{|m|}(\rho) - is_0\rho \exp\left[\frac{if}{u_0}(1-\sqrt{1-s_0^2\rho^2})\right] \times [J_{m+1}(2\pi r\rho)\exp(i\phi) - J_{m-1}(2\pi r\rho)\exp(-i\phi)]\rho d\rho, \quad (13)$$

where the quantity $\gamma = \pi R/\lambda$ is a proportionality constant. In the formulas above, the upper index of each field component is related to the polarization component of the light in the entrance pupil. The radial image plane coordinate r is expressed in units of λ/s_0, the diffraction unit in the image plane. The quantity f is the defocus parameter, related to the real-space axial coordinate z by

$$f = -\frac{2\pi u_0}{\lambda} z, \quad (14)$$

$$u_0 = 1 - \sqrt{1 - s_0^2}. \quad (15)$$

The integral expressions in Eqs. (11)–(13) have common characteristics and, when we use $[1-(1-s_0^2\rho^2)^{1/2}][1+(1-s_0^2\rho^2)^{1/2}] = s_0^2\rho^2$, the resulting electric field vector in the image space is given by

$$\mathbf{E}^x(r,\phi,f) = -i\gamma s_0^2 \exp\left(\frac{-if}{u_0}\right)\sum_{n,m} i^m \beta_{nm}^x \exp(im\phi) \begin{pmatrix} V_{nm,0} + \frac{s_0^2}{2}V_{nm,2}\exp(2i\phi) + \frac{s_0^2}{2}V_{nm,-2}\exp(-2i\phi) \\ -\frac{is_0^2}{2}V_{nm,2}\exp(2i\phi) + \frac{is_0^2}{2}V_{nm,-2}\exp(-2i\phi) \\ -is_0 V_{nm,1}\exp(i\phi) + is_0 V_{nm,-1}\exp(-i\phi) \end{pmatrix}. \quad (16)$$

Here we have introduced, for $j = -2, -1, 0, 1, 2$, the integral

$$V_{nm,j} = \int_0^1 \rho^{|j|}(1+\sqrt{1-s_0^2\rho^2})^{-|j|+1} \times \exp\left[\frac{if}{u_0}(1-\sqrt{1-s_0^2\rho^2})\right] \times R_n^{|m|}(\rho) J_{m+j}(2\pi r\rho)\rho d\rho. \quad (17)$$

The above integral shows a resemblance with a basic integral $V_{nm}(r,f)$ appearing in the scalar treatment of the diffraction problem as given in Refs. 5 and 6:

$$V_{nm}(r,f) = \int_0^1 \exp(if\rho^2) R_n^{|m|}(\rho) J_m(2\pi r\rho)\rho d\rho, \quad (18)$$

with the Bessel-series representation

$$V_{nm}(r,f) = \epsilon_m \exp(if)\sum_{l=1}^{\infty}(-2if)^{l-1} \times \sum_{j=0}^{p} v_{lj}\frac{J_{|m|+l+2j}(2\pi r)}{l(2\pi r)^l}. \quad (19)$$

In Eq. (19), we have $\epsilon_m = -1$ for odd $m < 0$ and $\epsilon_m = 1$ otherwise, and with $p = (n-|m|)/2$, $q = (n+|m|)/2$ the coefficients v_{lj} are given as

$$v_{lj} = (-1)^p(|m|+l+2j)\binom{|m|+j+l-1}{l-1}\binom{j+l-1}{l-1} \times \binom{l-1}{p-j} \Big/ \binom{q+l+j}{l} \quad (20)$$

for $l = 1, 2, \ldots$, $j = 0, 1, \ldots, p$. For accuracy within an absolute value of 10^{-6}, summation can be truncated after a maximum of $l = |3f|$ terms.

In the limiting case of a vanishing NA ($s_0 \to 0$), the expressions for the field components E_y and E_z result in a value of zero, and we observe that the field component E_x then yields the value corresponding to scalar diffraction.

In the general case, compared with $V_{nm}(r,f)$, the integrand of $V_{nm,j}(r,f)$ shows a more complicated dependence on ρ and f because of the appearance of $\rho^{|j|}$ and the other two factors containing s_0. Moreover, the upper index of the Zernike polynomial and the order of the Bessel function are not identical; this was an essential condition for arriving at the series expression for $V_{nm}(r,f)$. In Appendix B, we will show in detail how the integral $V_{nm,j}(r,f)$ can be written systematically as a series of integrals $V_{nm}(r,f)$ by finding a suitable expansion for the functions $\rho^{|j|}[1+(1-s_0^2\rho^2)^{1/2}]^{-|j|+1}\exp\{(if/u_0)[1-(1-s_0^2\rho^2)^{1/2}]\}$ in Eq. (17). Here we just outline the successive steps to be taken for finding the coefficients of the expansion.

- We start by formally writing

$$(1+\sqrt{1-s_0^2\rho^2})^{-|j|+1}\exp\left[\frac{if}{u_0}(1-\sqrt{1-s_0^2\rho^2})\right] = \exp(g_j + if_j\rho^2)\sum_{k=0}^{\infty} h_{kj} R_{2k}^0(\rho), \quad (21)$$

where the coefficients g_j and f_j are defined by requiring the best fit for the constant and the quadratic term in ρ. The series of Zernike polynomials with coefficients h_{kj} will be normally limited to a constant term h_{0j} close to unity, and a relatively small higher-order term h_{2j}. If the value of s_0, the geometrical NA, approaches a value

of, say, 0.90 or the defocus parameter exceeds the value of 2π, higher-order coefficients h_{kj} are needed.

• For the integral $V_{nm,j}(r, f)$ to be reduced to the analytically known result $V_{nm}(r, f)$, the upper index of the Zernike polynomial and the order of the Bessel function should be identical. To achieve this goal, we note that in general the following relationships between Zernike polynomials can be established:

$$\rho^{|j|}R_n^{|m|}(\rho) = \sum_{s=0}^{|j|} c_{n|m|js}R_{n+|j|-2s}^{|m|+j}(\rho). \tag{22}$$

These relations were already derived in Ref. 15 for $|j| = 1, 2$, and they are reproduced in Appendix B.

• Having determined the two or three new Zernike polynomials that we denote by $R_{n+|j|-2s}^{|m|+j}(\rho)$, we need to evaluate products of these Zernike polynomials with a general polynomial $R_{2k}^0(\rho)$ that appeared in the first step. We will write in Appendix B,

$$R_{2k}^0(\rho)R_{n+|j|-2s}^{|m|+j}(\rho) = \sum_{t=0}^{\infty} d_{n|m|jskt}R_{n+|j|-2s+2t}^{|m|+j}(\rho), \tag{23}$$

and we will show that the number of terms t in this summation is normally limited to three.

When the above steps are combined, it thus appears that $V_{nm,j}$ can be written as a linear combination of a modest number of terms of the form $V_{n+|j|-2s+2t,m+j}(r, f_j)\exp(g_j)$.

Having indicated the way to reduce the integrals $V_{nm,j}(r, f)$ to the known type $V_{nm}(r, f)$, we now return to the expressions for the electric field components. The y-polarized component E^y of the electric field in the entrance pupil yields an electric vector in image space according to

$$\mathbf{E}^y(r, \phi, f) = -i\gamma s_0^2 \exp\left(\frac{-if}{u_0}\right)\sum_{n,m} i^m \beta_{nm}^y \exp(im\phi)\begin{pmatrix} -\frac{is_0^2}{2}[V_{nm,2}\exp(2i\phi) - V_{nm,-2}\exp(-2i\phi)] \\ V_{nm,0} - \frac{s_0^2}{2}[V_{nm,2}\exp(2i\phi) + V_{nm,-2}\exp(-2i\phi)] \\ -s_0[V_{nm,1}\exp(i\phi) + V_{nm,-1}\exp(-i\phi)] \end{pmatrix}. \tag{24}$$

The magnetic induction components $\mathbf{B}$ are obtained from the electric components according to

$$\mathbf{B} = \frac{\mathbf{s} \times \mathbf{E}}{v}, \tag{25}$$

where $\mathbf{s}$ is the unit propagation vector from a point in the exit pupil to the focal plane and v is the speed of propagation of the light (equal to c in vacuum). Using Eq. (24), we write the magnetic induction vector components as

$$\mathbf{B}(r, \phi, f) = -\frac{in_r\gamma s_0^2}{c}\exp\left(\frac{-if}{u_0}\right)\sum_{n,m} i^m \exp(im\phi) \times \begin{pmatrix} -\beta_{nm}^y V_{nm,0} - \frac{s_0^2}{2}(\beta_{nm}^y + i\beta_{nm}^x)V_{nm,2}\exp(2i\phi) - \frac{s_0^2}{2}(\beta_{nm}^y - i\beta_{nm}^x)V_{nm,-2}\exp(-2i\phi) \\ \beta_{nm}^x V_{nm,0} - \frac{s_0^2}{2}(\beta_{nm}^x - i\beta_{nm}^y)V_{nm,2}\exp(2i\phi) - \frac{s_0^2}{2}(\beta_{nm}^x + i\beta_{nm}^y)V_{nm,-2}\exp(-2i\phi) \\ -s_0(\beta_{nm}^x - i\beta_{nm}^y)V_{nm,1}\exp(i\phi) - s_0(\beta_{nm}^x + i\beta_{nm}^y)V_{nm,-1}\exp(-i\phi) \end{pmatrix}, \tag{26}$$

where n_r denotes the refractive index of the dielectric medium.

Formal expressions for the electric energy density and the Poynting vector. When we focus our attention on the electric energy per unit volume in the focal region, we do not explicitly need the magnetic induction components. For light energy detection purposes (photographic plate, photoresist, CCD detector, etc.), the time-averaged value of the electric field energy density $\langle W_e\rangle$ has to be considered, and for a harmonic field in a homogeneous medium with a dielectric constant ϵ, this yields

$$\langle W_e\rangle = \frac{\epsilon_0}{4}n_r^2|\mathbf{E}|^2. \tag{27}$$

The electric field components from Eqs. (16) and (24) are used to compute the scalar product $\mathbf{E}^* \cdot \mathbf{E}$.

To examine the energy flow through the focal region, we have to evaluate the time-averaged values of the Cartesian components of the Poynting vector $\mathbf{S}$, and this leads to the expression

$$\langle \mathbf{S}\rangle = \frac{\epsilon_0 c^2}{2}\mathrm{Re}(\mathbf{E} \times \mathbf{B}^*). \tag{28}$$

Because of their lengths, we do not present here the explicit analytic expressions for $\langle W_e\rangle$ and $\langle \mathbf{S}\rangle$.

5. HIGH-NUMERICAL-APERTURE FOCAL FIELD DISTRIBUTIONS

In this section, we present some illustrative examples of the electromagnetic field distribution in the focal region that have been obtained with our analytic approach. We also briefly comment on the computational aspects of the method.

A. Focal Field Distributions

We start by considering the aberration-free case and a linear state of polarization in the entrance pupil. At low-NA values, a uniform amplitude and phase distribution in the exit pupil results in the well-known Airy distribution in the focal region. To study the high-NA effects in the aberration-free case, we first evaluate the Zernike coefficients due to the radiometric effect for a NA of 0.95 [see Eq. (7)]. To have an acceptable accuracy and demonstrate the strength of our method, we have considered Zernike coefficients with $m = 0$ and a maximum lower index up to $n = 16$, and up to $k = 12$ coefficients in the expansion of Eq. (7) [more exactly, $N = 4$ in Eq. (B26) of Appendix B and a third-order Taylor expansion of Eq. (B25)].

In Fig. 3, we have plotted the in-focus energy density at the high-NA value of 0.95 as a function of the radial coordinate r; the incident field is linearly polarized along the x axis ($\theta = 0$). The dotted curve corresponds to the energy density distribution along the x axis, and the dashed curve applies to the y axis ($\theta = \pi/2$). As a comparison, the scalar intensity distribution (Airy function) has been shown (solid curve). As is well-known from previous publications (e.g., Ref. 4), the distribution in the cross section with $\theta = 0$ is significantly broader than the Airy distribution. The calculations show that in the cross section $\theta = \pi/2$ the FWHM of the energy density function becomes slightly smaller than the FWHM of the Airy distribution and that the sidelobes are more pronounced. This would be consistent with the observation that the amplitude distribution on the exit pupil in terms of the radial coordinate ρ increases toward the rim of the pupil as a result of the radiometric effect.

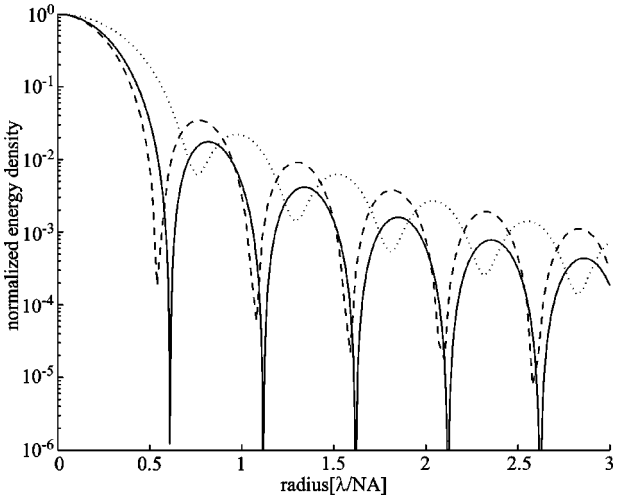

Fig. 3. Comparison of the energy density function in the high-NA focus ($f = 0$) and the scalar Airy distribution as a function of the radial coordinate r. The energy density function in the cross section $\theta = 0$ is represented by the dotted curve, and the one in the cross section $\theta = \pi/2$ by the dashed curve. The scalar Airy distribution is shown by the solid curve. The fact that the dashed high-aperture curve does not reach very low levels is due to the sampling density used in plotting this curve.

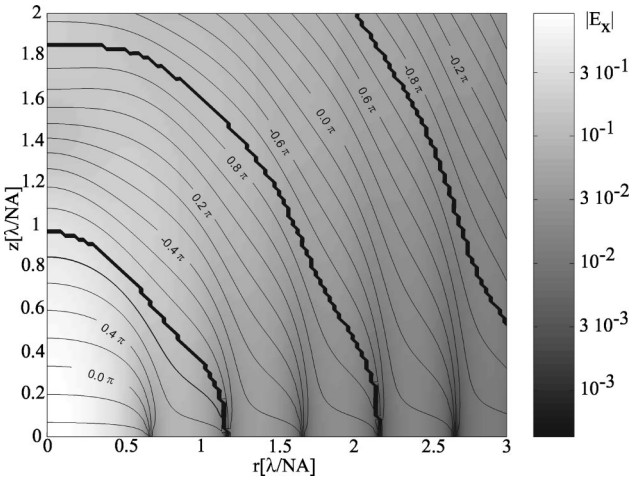

Fig. 4. Modulus of the x-polarization component of the electric field distribution in the focal region along the x axis ($\theta = 0$). The amplitude of the field component is indicated by a gray level on a logarithmic scale, and the contours denote equiphase lines. The radial coordinate r has been normalized with respect to the diffraction unit λ/s_0, and the axial coordinate with respect to the quantity u_0 [see Eq. (15)].

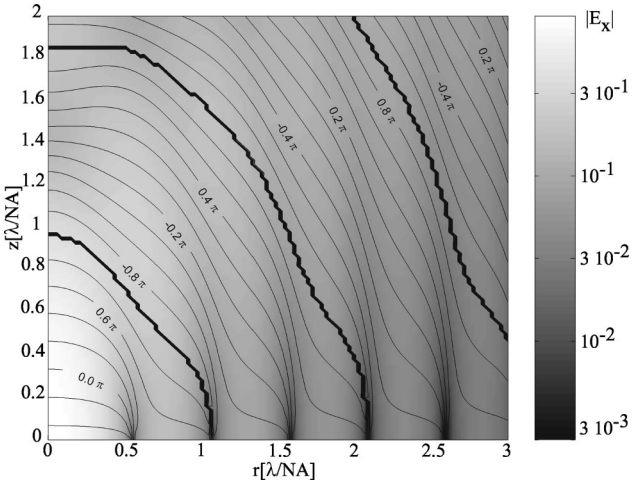

Fig. 5. Modulus of the x-polarization component of the electric field distribution in the focal region along the y axis ($\theta = \pi/2$). The amplitude of the field component is indicated by a gray level on a logarithmic scale, and the contours denote equiphase lines.

We also executed a numerical evaluation of the solution as given by Ref. 4 and compared this result with our quasi-analytic solution. A discrepancy of less than 10^{-6} in intensity was observed, depending on the point density when carrying out the numerical integration.

In Figs. 4 and 5, we show the logarithm of the modulus of the x component of the electric field along, respectively, the x and y axes (the incident field is polarized along the x axis). Considering the positions of the first zeros in the focal plane along the x and y axes, we again observe a ratio of the widths of these energy density cross sections of

typically 80%. As we noted above, this asymmetric effect is well-known and has been numerically evaluated before.[4,16]

In Figs. 6 and 7, the corresponding y and z components (moduli) of the electric field have been shown along the diagonal $x = y$ and the x axis, respectively. As expected, the electric field on the optical axis is zero.

The next example applies to an entrance pupil distribution with a radially oriented linear state of polarization in each point; the modulus of the amplitude and the phase of the wave are uniform. The resulting Poynting vector distribution is shown in Fig. 8. The Zernike coefficients describing the electric field in the exit pupil have been given in Eq. (7). Again, the NA is as high as 0.95. It is interesting to note that the Poynting vector distributions for azimuthally and radially polarized light distributions in the entrance pupil are identical. This is understood by the interchangeability of the electric field and the magnetic induction for the radial and azimuthal linear polarization states.

The third example is related to the helical phase distribution as defined by the coefficients calculated in Eq. (9).

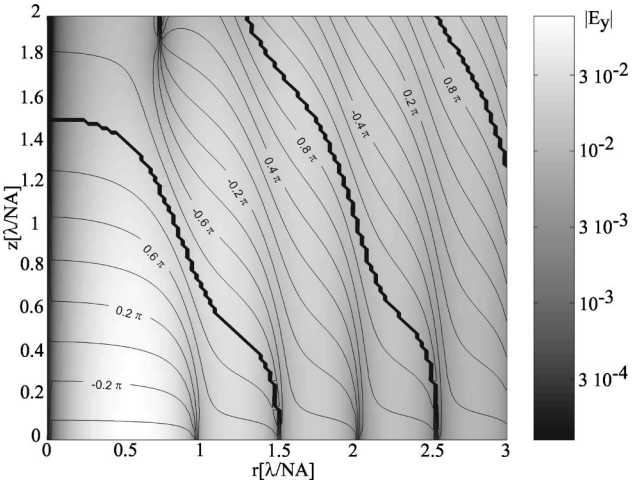

Fig. 6. Modulus of the y-polarization component of the electric field distribution in the focal region along the diagonal $x = y$ ($\theta = \pi/4$).

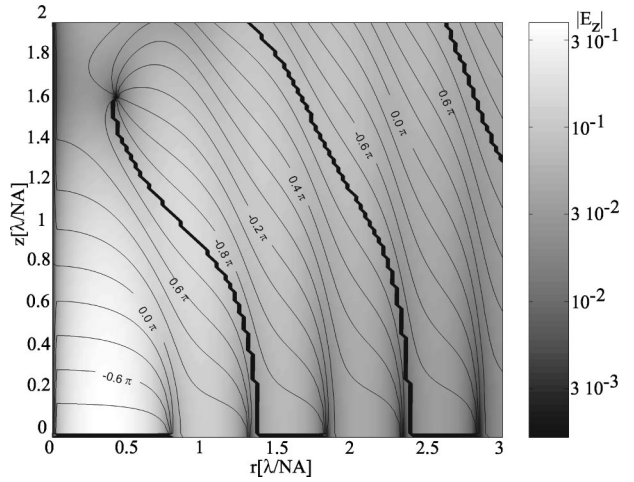

Fig. 7. Modulus of the z-polarization component of the electric field distribution in the focal region along the x axis ($\theta = 0$).

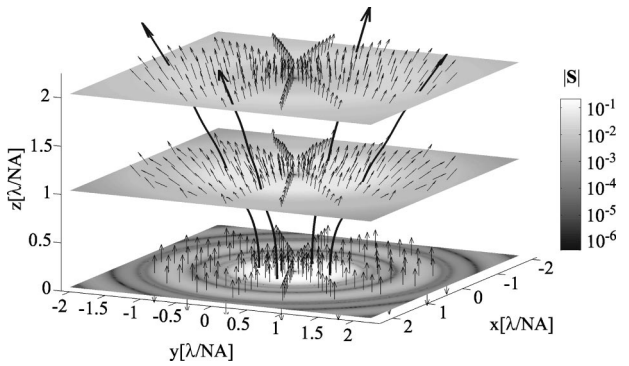

Fig. 8. A radially polarized entrance pupil distribution yields a radially symmetric Poynting vector distribution in the focal region. The absolute value of the Poynting vector is indicated by a gray level on a logarithmic scale, and its direction is given by a set of arrows. Note that the value in the geometrical focus equals zero.

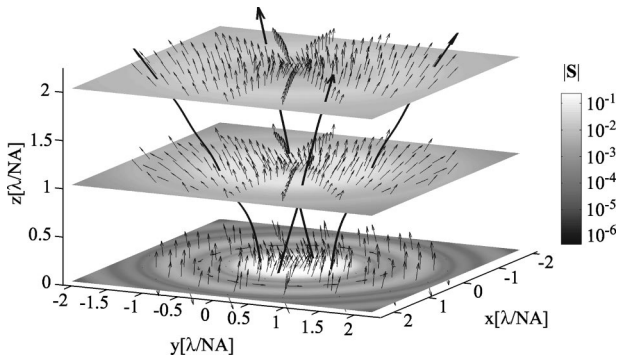

Fig. 9. A helical phase distribution in the presence of a linear polarization state in the entrance pupil yields a rotating Poynting vector field in the focal region. The absolute value of the Poynting vector is indicated by a gray level on a logarithmic scale, and its direction is given by a set of arrows.

The helical structure of the incoming wave front carries orbital angular momentum, and from Fig. 9 it can be concluded that this angular momentum is still present in the focal plane (a detailed analysis should show that it is effectively preserved). The Poynting vector distribution is given for a 0.95-NA imaging system.

It can be proven that, within the approximations of the model and for the chosen aberrations, all shown distributions are symmetric either with respect to the focal plane or with respect to the geometrical focal point; therefore we have chosen to plot only the values along the positive z axis.

B. Further Aspects of Our Approach

We have not yet optimized our computational schemes with respect to computation time; neither have we yet made an extensive comparison in this respect with existing numerical software packages. For a list of advantages of our analytic approach over strictly numerical methods, we refer to Ref. 6 (Subsec. 4.B). In particular, we may point out that the variables and the coefficients r, ϕ, f, and β all occur in a separated form in our formulas for the field components. This means, for instance, that the computational load is reduced substantially when one or more of the variables r, ϕ, and f is fixed. Our method

for evaluating the Zernike coefficients is based on the computation of individual inner products. More efficient and stable methods employing global Fourier techniques are possible but have not been implemented yet.[17] We intend to use these potential high-speed computational methods so as to achieve near-real-time three-dimensional visualization of the focal fields such as that shown in Figs. 4–9. Varying states of polarization and aberration could be effectively handled by fully exploiting the basic separation of variables and coefficients in our analysis.

Finally, we would like to draw attention to another aspect of our analysis: the explicit dependence of, e.g., the field energy density on our β coefficients. The latter represent the particularities of the optical system, e.g., its aberration and transmission nonuniformity. In Ref. 7, a method has been pointed out to retrieve the aberrational data of an optical system from the through-focus intensity distribution. This method is based on a scalar treatment of the diffraction problem, but the radiometric effect arising at high-NA values can be included (see Ref. 8). The method is based on the Zernike expansion of the unknown complex pupil function, whose coefficients have to be found by a matching procedure. In a future paper, we will extend the method from Ref. 8 to the fully vectorial diffraction problem. The method being based again on a matching of the β coefficients, it can be conceived only in an analytic framework such as the one that we have described in this paper.

6. CONCLUSIONS

We have demonstrated that it is possible to extend an analytic result applying to Nijboer–Zernike diffraction integrals from the scalar case to the fully vectorial case. The radiometric amplitude effects, the wave aberration, and the polarization state of the wave in the exit pupil are included in an analytic procedure that makes multiple use of our "extended" Nijboer–Zernike expression for the diffraction integral. Two sets of complex Zernike coefficients, one for each orthogonal state of polarization, is sufficient to describe the electromagnetic field in the focal region.

The feasibility of our method is proven by the calculation of extremely high-NA examples over a large range of both the radial as well as the axial coordinate. Although the examples in this paper do not contain a large amount of aberration, the Zernike coefficients describing the system have large values of the indices n and m, caused by the inclusion of the radiometric effect. Practical limits for the radial and total axial excursion are of the order of 20 diffraction units in both orthogonal directions; a simple convergence criterion determines to what extent the analytic series expansion of the diffraction integral has to be continued.

A comparison of computational speed between our analytic approach and purely numerical methods has been planned for the near future. We also intend to further exploit the analytic nature of our solution in order to obtain a retrieval scheme for the aberration and transmission defects of an optical system with use of the complex Zernike coefficients. Earlier work on a retrieval scheme for the scalar diffraction problem has shown promising results; the next step is its extension to the fully vectorial case.

APPENDIX A: RADIOMETRIC EFFECT AND ZERNIKE INTEGRALS

In this appendix, we evaluate the integral

$$I_{m+2p}^{m} = \int_0^1 \frac{R_{m+2p}^{m}(\rho)}{(1 - s_0^2\rho^2)^{1/4}}\rho \mathrm{d}\rho, \qquad m, \ p = 0, \ 1,..., \tag{A1}$$

in a form that is convenient for numerical computation.

We start from the result, valid for $\alpha > -1$,

$$\int_0^1 \rho^{\alpha} R_{m+2p}^{m}(\rho)\rho \mathrm{d}\rho = \frac{1}{2}(-1)^p \frac{(\tfrac{1}{2}m - \tfrac{1}{2}\alpha)_p}{(\tfrac{1}{2}m + \tfrac{1}{2}\alpha + 1)_{p+1}}, \tag{A2}$$

where we have used Pochhammer's symbol [see Ref. 18, Eq. (6.1.21), p. 256]:

$$(a)_0 = 1, \qquad (a)_n = a(a + 1) \times \cdots \times (a + n - 1), \qquad n = 1, \ 2,.... \tag{A3}$$

This result is readily proven as follows. It is well known (see Ref. 14, Appendix VII, Sec. 2) that

$$R_{m+2p}^{m}(\rho) = \rho^m P_p^{(0,m)}(2\rho^2 - 1), \tag{A4}$$

where $P_k^{(\alpha,\beta)}$ is the Jacobi polynomial in the notation of Ref. 19 (Chap. 4). Substituting $z = 2\rho^2 - 1$ into the integral in Eq. (A2) and noting the Rodrigues formula

$$P_p^{(0,m)}(z) = \frac{(-1)^p}{2^p p!}\left(\frac{\mathrm{d}}{\mathrm{d}z}\right)^p [(1 - z)^p(1 + z)^{p+m}], \tag{A5}$$

we obtain Eq. (A2) by p partial integrations and some administration.

From the Taylor expansion of $(1 - x)^{-1/4}$ around $x = 0$,

$$(1 - x)^{-1/4} = \sum_{k=0}^{\infty} \frac{(\tfrac{1}{4})_k}{k!}x^k, \tag{A6}$$

it follows from Eq. (A2) that

$$I_{m+2p}^{m} = \sum_{k=0}^{\infty} \frac{(\tfrac{1}{4})_k}{k!} s_0^{2k} \int_0^1 \rho^{2k} R_{m+2p}^{m}(\rho)\rho \mathrm{d}\rho = \frac{1}{2}(-1)^p \sum_{k=0}^{\infty} \frac{(\tfrac{1}{4})_k}{k!} \frac{(\tfrac{1}{2}m - k)_p}{(\tfrac{1}{2}m + k + 1)_{p+1}} s_0^{2k}. \tag{A7}$$

We observe that

$$0 \leqslant \frac{(\tfrac{1}{4})_k}{k!} \leqslant \frac{1}{\Gamma(\tfrac{1}{4})k^{3/4}}, \qquad k = 1, \ 2,..., \tag{A8}$$

and that

$$\left|\frac{(\frac{1}{2}m-k)_p}{(\frac{1}{2}m+k+1)_{p+1}}\right| \leqslant \frac{1}{k+\frac{1}{2}m+p+1}, \qquad k,\ m,\ p = 0,\ 1,\ldots. \tag{A9}$$

Hence when s_0 is not very close to 1, a modest number of terms in Eq. (A7) is required for accurate evaluation of I^m_{m+2p}.

From Eq. (A7), the integrals in Eqs. (7), (8), and (10) are readily obtained in a numerically convenient form.

APPENDIX B: REDUCTION OF INTEGRALS TO BASIC FORM

In this appendix, we give the detailed derivation that is needed to transform the integral $V_{nm,j}(r, f)$ into a series of integrals $V_{nm}(r, f)$.

We shall first show that

$$\sqrt{1-s_0^2\rho^2} = -\frac{1}{2}u_0\sum_{n=0}^{\infty}\left(\frac{d_0^{n-1}}{2n-1}-\frac{d_0^{n+1}}{2n+3}\right)\times R^0_{2n}(\rho), \tag{B1}$$

$$\ln(1+\sqrt{1-s_0^2\rho^2}) = \frac{1}{2}d_0+\ln\left(\frac{u_0}{d_0}\right)-\frac{1}{2}\sum_{n=1}^{\infty}\left(\frac{d_0^n}{n}-\frac{d_0^{n+1}}{n+1}\right)R^0_{2n}(\rho), \tag{B2}$$

where

$$u_0 = 1-\sqrt{1-s_0^2}, \tag{B3}$$

$$d_0 = \left(\frac{u_0}{s_0}\right)^2. \tag{B4}$$

For this we use the generating functions of R^0_{2n} and R^1_{2n+1} in the form

$$\sum_{n=0}^{\infty} z^n R^0_{2n}(\rho) = \frac{1}{\sqrt{(1+z)^2-4z\rho^2}}, \tag{B5}$$

$$\sum_{n=0}^{\infty} z^n R^1_{2n+1}(\rho) = \frac{2\rho}{\sqrt{(1+z)^2-4z\rho^2}[1+z+\sqrt{(1+z)^2-4z\rho^2}]} \tag{B6}$$

[see Ref. 14, Appendix VII, Eq. (30), p. 771]. We may note here that the generating function as given in Ref. 14 [Sec. 9.2, Eq. (7), p. 465] is incorrect because of two minus signs that should be plus signs. By taking $z = d_0$, so that

$$\frac{4z}{(1+z)^2} = s_0^2, \tag{B7}$$

we can write Eq. (B5) as

$$\frac{\rho}{\sqrt{1-s_0^2\rho^2}} = (1+d_0)\sum_{n=0}^{\infty} d_0^n\rho R^0_{2n}(\rho), \tag{B8}$$

and we can write Eq. (B6) as

$$\frac{\mathrm{d}}{\mathrm{d}\rho}[\ln(1+\sqrt{1-s_0^2\rho^2})] = \frac{-s_0^2\rho}{\sqrt{1-s_0^2\rho^2}(1+\sqrt{1-s_0^2\rho^2})} = -2d_0\sum_{n=0}^{\infty} d_0^n R^1_{2n+1}(\rho). \tag{B9}$$

By integrating Eq. (B8) from 0 to ρ, we get

$$\frac{1}{s_0^2}(1-\sqrt{1-s_0^2\rho^2}) = (1+d_0)\sum_{n=0}^{\infty} d_0^n\int_0^{\rho}\varrho R^0_{2n}(\varrho)\mathrm{d}\varrho, \tag{B10}$$

and by integrating Eq. (B9) from ρ to 1, we get

$$\ln(1+\sqrt{1-s_0^2\rho^2})-\ln\left(\frac{u_0}{d_0}\right) = 2d_0\sum_{n=0}^{\infty} d_0^n\int_{\rho}^{1} R^1_{2n+1}(\varrho)\mathrm{d}\varrho. \tag{B11}$$

It remains to evaluate the integrals

$$\int_0^{\rho}\varrho R^0_{2n}(\varrho)\mathrm{d}\varrho, \qquad \int_{\rho}^{1} R^1_{2n+1}(\varrho)\mathrm{d}\varrho. \tag{B12}$$

As to the first integral in expression (B12), we note that $R^0_{2n}(\varrho) = P_n(2\varrho^2-1)$, with P_n as the nth Legendre polynomial. By Ref. 20 [Eq. (10.10), p. 190], we have

$$(2n+1)P_n(x) = P'_{n+1}(x)-P'_{n-1}(x), \qquad n = 1,\ 2,\ldots. \tag{B13}$$

Hence

$$\int_0^{\rho}\varrho R^0_{2n}(\varrho)\mathrm{d}\varrho = \frac{1}{4(2n+1)}[R^0_{2n+2}(\rho)-R^0_{2n-2}(\rho)] \tag{B14}$$

for $n = 1, 2,\ldots$, where we have used that $R^0_{2n+2}(0) = R^0_{2n-2}(0) = (-1)^{n+1}$. Also,

$$\int_0^{\rho}\varrho R^0_0(\varrho)\mathrm{d}\varrho = \frac{1}{2}\rho^2 = \frac{1}{4}[R^0_2(\rho)+R^0_0(\rho)]. \tag{B15}$$

As to the second integral in expressions (B12), we note Ref. 15 [Eq. (2.32), p. 30], which implies that

$$R^1_{2n+1}(\rho) = \frac{1}{4(n+1)}\frac{\mathrm{d}}{\mathrm{d}\rho}[R^0_{2n+2}(\rho)-R^0_{2n}(\rho)] \tag{B16}$$

for $n = 0,\ 1,\ldots$. Hence

$$\int_{\rho}^{1} R^1_{2n+1}(\varrho)\mathrm{d}\varrho = \frac{-1}{4(n+1)}[R^0_{2n+2}(\rho)-R^0_{2n}(\rho)] \tag{B17}$$

for $n = 0,1,...$, where we have used that $R^0_{2n+2}(1) = R^0_{2n}(1) = 1$. Inserting Eqs. (B14) and (B15) into Eq. (B10) and Eq. (B17) into Eq. (B11), we easily obtain the results in Eqs. (B1) and (B2).

1. Step I

Using the results obtained in the derivation above, we first write

$$(-|j| + 1)\ln(1 + \sqrt{1 - s_0^2\rho^2}) + \frac{if}{u_0}(1 - \sqrt{1 - s_0^2\rho^2}) = (-|j| + 1)\sum_{n=0}^{\infty} b_n R^0_{2n}(\rho) + if\sum_{n=0}^{\infty} a_n R^0_{2n}(\rho) = g_j + if_j\rho^2 + \sum_{n=2}^{\infty} \tau_{nj} R^0_{2n}(\rho). \quad \text{(B18)}$$

The various coefficients are given by

$$a_0 = \frac{1}{2} - \frac{1}{6}d_0,$$

$$a_n = \frac{1}{2}\left(\frac{d_0^{n-1}}{2n - 1} - \frac{d_0^{n+1}}{2n + 3}\right), \qquad n = 1, 2,..., \quad \text{(B19)}$$

$$b_0 = \frac{1}{2}d_0 + \ln\left(\frac{u_0}{d_0}\right),$$

$$b_n = -\frac{1}{2}\left(\frac{d_0^n}{n} - \frac{d_0^{n+1}}{n + 1}\right), \qquad n = 1, 2,..., \quad \text{(B20)}$$

$$g_j = (-|j| + 1)(b_0 - b_1) + if(a_0 - a_1), \quad \text{(B21)}$$

$$f_j = 2fa_1 - 2i(-|j| + 1)b_1, \quad \text{(B22)}$$

$$\tau_{nj} = (-|j| + 1)b_n + ifa_n, \qquad n = 2, 3,.... \quad \text{(B23)}$$

For the original expression, we now obtain

$$(1 + \sqrt{1 - s_0^2\rho^2})^{-|j|+1} \exp\left[\frac{if}{u_0}(1 - \sqrt{1 - s_0^2\rho^2})\right] = \exp(g_j + if_j\rho^2)G_j(\rho), \quad \text{(B24)}$$

with

$$G_j(\rho) = \exp\left[\sum_{n=2}^{\infty} \tau_{nj} R^0_{2n}(\rho)\right]. \quad \text{(B25)}$$

We remark that the function $G_j(\rho)$ is what remains after splitting off an exponential factor consisting of the best quadratic approximation to the left-hand-side function of ρ in Eq. (B18). Consequently, the remaining summation can be expected to be numerically small, typically significantly less than unity. In that case, we write

$$G_j(\rho) \approx 1 + \sum_{n=2}^{N} \tau_{nj} R^0_{2n}(\rho), \qquad N = 2, 3, \text{ or } 4. \quad \text{(B26)}$$

Inspection of Eq. (B23) shows that the coefficients τ_{nj} depend linearly on f and in a more complicated way on s_0. For large values of s_0 and large f, it may be necessary to include the quadratic term

$$\frac{1}{2}\left[\sum_{n=2}^{N} \tau_{nj} R^0_{2n}(\rho)\right]^2 \quad \text{(B27)}$$

into the approximation of $G_j(\rho)$. This occurs only for s_0 as large as 0.90 and $|f| = 2\pi$ or larger. In that case, one may use the formula (Ref. 21, Corollary 6.8.3, p. 320)

$$R^0_{2n'}R^0_{2n} = \sum_{r=0}^{n'} \frac{A_{n'-r}A_rA_{n-r}}{A_{n'+n-r}} \frac{2n' + 2n - 4r + 1}{2n' + 2n - 2r + 1} R^0_{2n'+2n-4r}, \quad \text{(B28)}$$

for $0 \leqslant n' \leqslant n$ with

$$A_n = \frac{1}{n!}[1 \times 3 \times \cdots \times (2n - 1)] = \frac{1}{2^n}\binom{2n}{n}, \quad \text{(B29)}$$

to write the products of Zernike polynomials with upper index zero in Eq. (B24) as linear combinations of these Zernike polynomials. Note that now the expansion coefficients of G_j depend quadratically on f. The function G_j can of course also be expanded directly into a Zernike series ($n = 0$), but then the dependence of the coefficients on f is awkward.

2. Step II

To reduce the expressions for the field components to a form that is analytically tractable, we need to be able to adapt the upper index $m \geqslant 0$ of Zernike polynomials according to the recursion formulas given by Nijboer.[15] The starting point is the formulas

$$\rho R^m_n(\rho) = \frac{q + 1}{n + 1} R^{m+1}_{n+1}(\rho) + \frac{p}{n + 1} R^{m+1}_{n-1}(\rho), \quad \text{(B30)}$$

$$\rho R^m_n(\rho) = \frac{p + 1}{n + 1} R^{m-1}_{n+1}(\rho) + \frac{q}{n + 1} R^{m-1}_{n-1}(\rho), \quad \text{(B31)}$$

where, as usually, $p = (n - m)/2$ and $q = (n + m)/2$, which permit us to raise or to lower the upper index by one unit. A straightforward calculation yields the expressions to induce a change of ± 2 in the upper index:

$$\rho^2 R^m_n(\rho) = \frac{(p + 1)(p + 2)}{(n + 1)(n + 2)} R^{m-2}_{n+2}(\rho) + \frac{2(p + 1)q}{n(n + 2)} R^{m-2}_n(\rho) + \frac{q(q - 1)}{n(n + 1)} R^{m-2}_{n-2}(\rho), \quad \text{(B32)}$$

$$\rho^2 R_n^m(\rho) = \frac{(q+1)(q+2)}{(n+1)(n+2)} R_{n+2}^{m+2}(\rho) + \frac{2p(q+1)}{n(n+2)} R_n^{m+2}(\rho) + \frac{p(p-1)}{n(n+1)} R_{n-2}^{m+2}(\rho). \tag{B33}$$

The coefficients $c_{n|m|js}$ in Section 4 are easily extracted from the formulas above.

3. Step III

We finally need to write any product $R_{2k}^0 R_n^m$ as a linear combination of R_{n+2t}^m. From the formulas above and with $R_2^0(\rho) = 2\rho^2 - 1$, we derive

$$R_2^0(\rho) R_n^m(\rho) = 2\frac{(p+1)(q+1)}{(n+1)(n+2)} R_{n+2}^m(\rho) + \frac{m^2}{n(n+2)} R_n^m(\rho) + 2\frac{pq}{n(n+1)} R_{n-2}^m(\rho), \tag{B34}$$

with, again, $p = (n-m)/2$ and $q = (n+m)/2$.

Higher-order polynomials $R_{2k}^0(\rho)$ can be written as a polynomial having the argument $R_2^0(\rho) = 2\rho^2 - 1$, according to

$$R_{2k}^0(\rho) = P_k[R_2^0(\rho)] = \sum_{l=0}^{[k/2]} \frac{(-1)^l}{2^k} \binom{k}{l} \binom{2k-2l}{k} \times [R_2^0(\rho)]^{k-2l}. \tag{B35}$$

Here P_k is the kth Legendre polynomial, and $[k/2]$ is the largest integer $\leqslant k/2$. Using Eq. (B35) and then Eq. (B34) repeatedly, we can write any product $R_{2k}^0(\rho) R_n^m(\rho)$ as a linear combination of at most $2k+1$ terms $R_{n+2t}^m(\rho)$. Accordingly, in general, we can write

$$R_{2k}^0(\rho) R_{n+|j|-2s}^{|m|+j}(\rho) = \sum_t d_{n|m|jskt} R_{n+|j|-2s+2t}^{|m|+j}(\rho). \tag{B36}$$

In practice, we will observe that the number of required terms in the series $\Sigma_k h_{kj} R_{2k}^0(\rho)$ on the right-hand side of Eq. (21) is limited to $k = 2$ and that we have to proceed to values of $k = 3$ or 4 only at extremely high values of the NA or at very large defocusing values. Therefore the computational task does not get out of hand in practical cases.

ACKNOWLEDGMENT

Part of this research has been carried out in the framework of the European project IST-2000-26479 (SLAM).

The authors can be reached by e-mail at j.j.m.braat@tnw.tudelft.nl, peter.dirksen@philips.com, a.j.e.m.janssen@philips.com, and a.vandenes@tnw.tudelft.nl.

REFERENCES

1. B. H. W. Hendriks, J. J. H. B. Schleipen, S. Stallinga, and H. van Houten, "Optical pickup for blue optical recording at NA = 0.85," Opt. Rev. **8**, 211–213 (2001).
2. H. P. Urbach and D. A. Bernard, "Modeling latent-image formation in the photolithography, using the Helmholtz equation," J. Opt. Soc. Am. A **6**, 1343–1356 (1989).
3. V. S. Ignatowsky, "Diffraction by a lens of arbitrary aperture," Tr. Opt. Inst. **1** (4), 1–36 (1919).
4. B. Richards and E. Wolf, "Electromagnetic diffraction in optical systems II. Structure of the image field in an aplanatic system," Proc. R. Soc. London Ser. A **253**, 358–379 (1959).
5. A. J. E. M. Janssen, "Extended Nijboer–Zernike approach for the computation of optical point-spread functions," J. Opt. Soc. Am. A **19**, 849–857 (2002).
6. J. J. M. Braat, P. Dirksen, and A. J. E. M. Janssen, "Assessment of an extended Nijboer–Zernike approach for the computation of optical point-spread functions," J. Opt. Soc. Am. A **19**, 858–870 (2002).
7. P. Dirksen, J. J. M. Braat, A. J. E. M. Janssen, and C. Juffermans, "Aberration retrieval using the extended Nijboer–Zernike approach," J. Microlithogr. Microfabr. Microsyst. **2**, 61–68 (2003).
8. J. J. M. Braat, P. Dirksen, and A. J. E. M. Janssen, "Retrieval of aberrations from intensity measurements in the focal region using an extended Nijboer–Zernike approach," manuscript available from the author, j.j.m.braat@tnw.tudelft.nl.
9. N. R. Heckenberg, T. A. Nieminen, M. E. J. Friese, and H. Rubinsztein-Dunlop, "Trapping microscopic particles with singular beams," in *International Conference on Singular Optics*, M. S. Soskin, ed., Proc. SPIE **3487**, 46–53 (1998).
10. L. Allen, M. W. Beijersbergen, R. J. C. Spreeuw, and J. P. Woerdman, "Orbital angular momentum of light and the transformation of Laguerre–Gaussian laser modes," Phys. Rev. A **45**, 8185–8189 (1992).
11. L. Allen, J. Courtial, and M. J. Padgett, "Matrix formulation for the propagation of light beams with orbital and spin angular momenta," Phys. Rev. E **60**, 7497–7503 (1999).
12. W. Welford, *Aberrations of Optical Systems* (Hilger, Bristol, UK, 1986).
13. S. Stallinga, "Axial birefringence in high-numerical-aperture optical systems and the light distribution close to focus," J. Opt. Soc. Am. A **18**, 2846–2859 (2001).
14. M. Born and E. Wolf, *Principles of Optics*, 4th ed. (Pergamon, New York, 1970).
15. B. R. A. Nijboer, "The diffraction theory of aberrations," Ph.D. thesis (University of Groningen, Groningen, The Netherlands, 1942).
16. P. Török, P. Varga, and G. Nemeth, "Analytical solution of the diffraction integrals and interpretation of wave-front distortion when light is focused through a planar interface between materials of mismatched refractive indices," J. Opt. Soc. Am. A **12**, 2660–2671 (1995).
17. A. J. E. M. Janssen, "Stable representation of Zernike polynomials," Internal Rep. NL TN, 2001/263 (Philips Research Laboratories, Eindhoven, The Netherlands, 2002).
18. M. Abramowitz and I. A. Stegun, *Handbook of Mathematical Functions* (Dover, New York, 1970).
19. G. Szegő, *Orthogonal Polynomials*, 4th ed. (American Mathematical Society, Providence, 1975).
20. F. G. Tricomi, *Vorlesungen über Orthogonalreihen* (Springer, Berlin, 1955).
21. G. E. Andrews, R. Askey, and R. Roy, *Special Functions* (Cambridge U. Press, Cambridge, UK, 1999).